Science & Technology Development Journal 2023, 26(4):3225-3243

Open Access Full Text Article

Engineering and Technology: Research Article

Aerodynamic Property Investigation of an Unmanned Aerial Vehicle (UAV) in the Case of Forward Flight by a Numerical Approach

Tien Nghi Nguyen[1,*], Thi Hong Hieu Le[1], Ngoc Hien Nguyen[2]

ABSTRACT

In the golden era of digitalization, flow calculation research based on a numerical approach has become increasingly popular in the scientific world and has played a vital role in revealing the aerodynamic characteristics of various aircraft models. This paper, belonging to computational fluid dynamics, describes the process and results of a numerical simulation approach using the software OpenFOAM for an unmanned aerial vehicle (UAV) in the case of forwarding flight with a low Reynolds number. With regard to the numerical approach, the aerodynamic properties are investigated through the turbulence model k-ω-SST (shear stress transport), which is a part of the turbulence calculation approach Reynolds average Navier–Stokes (RANS). Furthermore, the entire process of mesh generation and the numerical calculation process by simpleFoam in OpenFOAM, which is the solver using the semi-implicit method for pressure-linked equations (SIMPLE) algorithm for steady, incompressible flow, are also depicted in this paper. In addition, the characteristics of the flow field surrounding the model and the characteristic aerodynamic coefficients (drag coefficient, lift coefficient, lift-to-drag ratio versus angle of attack and pressure coefficients, and skin-friction coefficients for special positions on the wing) of the model are also clearly illustrated. Finally, the simulation illustrations in ParaView, including the velocity field, pressure field and vortices in the stagnation region, are shown. The process description and results contribute a clear picture of the numerical execution steps in OpenFOAM and aerodynamic knowledge for a particular unmanned aerial vehicle model to the computational fluid dynamics field in the aerospace industry.

Key words: Forward flight, OpenFOAM, SIMPLE, RANS, k-ω-SST

[1]*Department of Aerospace Engineering, Ho Chi Minh City University of Technology (HCMUT) – Vietnam National University (VNU), Ho Chi Minh City, Viet Nam*

[2]*Ngoc Hien Nguyen is with the Department of Mathematical Sciences, RMIT University, Australia*

Correspondence

Tien Nghi Nguyen, Department of Aerospace Engineering, Ho Chi Minh City University of Technology (HCMUT) – Vietnam National University (VNU), Ho Chi Minh City, Viet Nam

Email: nguyentiennghi212@gmail.com

History

- Received: 2019-07-30
- Accepted: 2023-11-20
- Published Online: 2024-12-31

DOI :

https://doi.org/10.32508/stdj.v26i4.1699

INTRODUCTION

Following the strong development trends in the aeronautic industry, unmanned aerial vehicles are becoming one of the most popular types of aircraft because of their flexibility, capacity to be controlled without a pilot and usefulness for multiple purposes. In fact, many studies have been devoted to designing new concepts according to the actual conditions for this type of aircraft and investigating the aerodynamic properties of existing UAV models. Therefore, from that point of view, it is sensible that the ex-student Huynh Tri Pham[2], in our department (the Department of Aerospace Engineering) of Ho Chi Minh City University of Technology, designed a UAV model during his graduation thesis in 2015. It is a hybrid UAV model that is a combination of a tricopter and a rectangular wing. Afterwards, in 2018, another ex-student, Duc Thanh Nguyen[1], created a new UAV model based on the Huynh Tri Pham model by changing the wingspan from 1.2 meters to 1.35 meters and the initial incidence angle from 0° to 4°. As a result, in comparison to the former model, the latter model has an aspect ratio that increases from 8 to 9 and a reference area that expands from 0.18 m^2 to 0.2025 m^2. The summary specifications of the two models are illustrated in the following picture and table:

In fact, the ex-student Huynh Tri Pham created the former model on the basis of aircraft design methods, while the ex-student Duc Thanh Nguyen generated this model on the basis of structural aspects. Moreover, the Huynh Tri Pham model was examined experimentally in the wind tunnel of our department. Nonetheless, until the end of 2018, there was still no simulation project to investigate the aerodynamic properties of both models entirely by a numerical approach. Therefore, it is reasonable that the objective of this study was to numerically examine the aerodynamic characteristics and compare both models. Furthermore, to clarify the results, in this paper, the author has also included the former results from another student's simulation analysis[3], which was conducted for two-dimensional airfoils utilized for these models.

Cite this article : Nguyen T N, Le T H H, Nguyen N H. **Aerodynamic Property Investigation of an Unmanned Aerial Vehicle (UAV) in the Case of Forward Flight by a Numerical Approach**. *Sci. Tech. Dev. J.* 2023; 26(4):3225-3243.

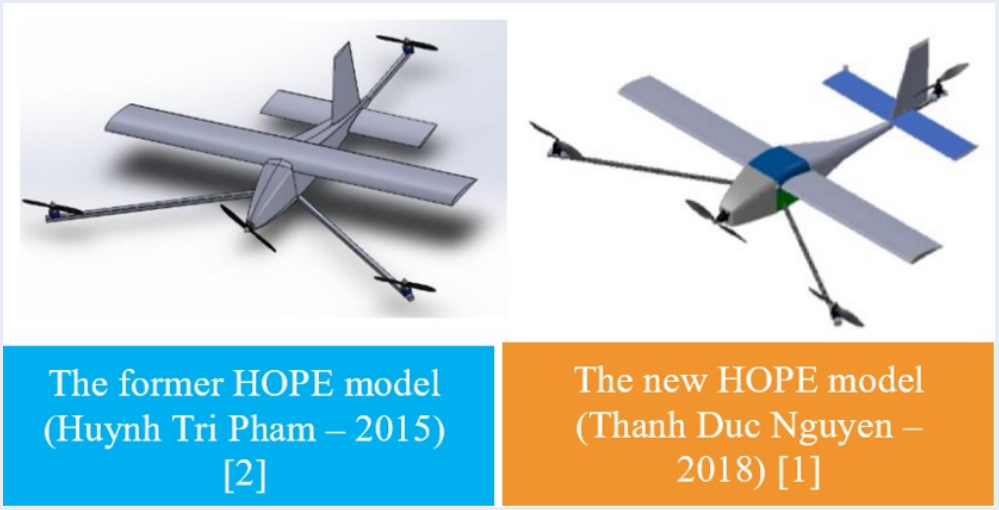

Figure 1: **The UAV models of Huynh Tri Pham in 2015 and Thanh Duc Nguyen in 2018** [1,2]

Table 1: **The specification summary chart of the two models**

	The former HOPE model (Huynh Tri Pham - 2015)	The new HOPE model (Duc Thanh Nguyen - 2018)
Airfoil type	BE12355d	BE12355d
Wing chord, c	0.15 m	0.15 m
Bar profile	square	circle
Wingspan	1.2 m	1.35 m
Reference Area	0.18 m^2	0.2025 m^2
Aspect ratio	8	9
Incidence angle, i_w	0°	4°

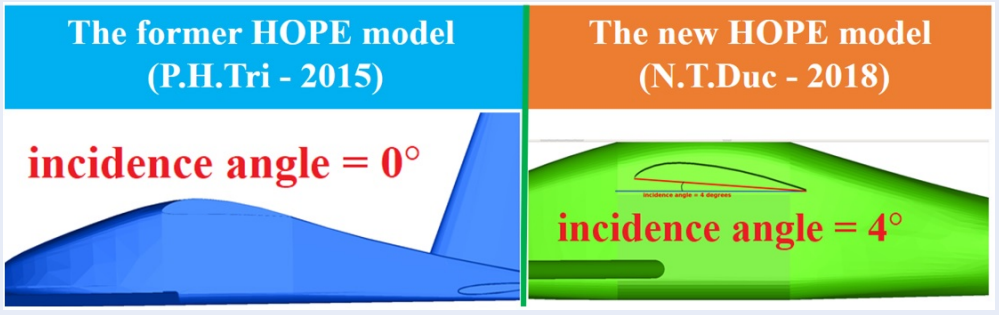

Figure 2: **The difference in the initial incidence angle between the two models.**

Moreover, in particular, in this numerical research, the model was executed at a velocity of 15 $m.s^{-1}$, a density of 1.225 $kg.m^{-3}$, and a viscosity of 1.81×10^{-5} $kg.m^{-1}.s^{-1}$. The density and viscosity are chosen following the conditions at sea level. As a result, the Renoyld number was calculated to be approximately 1.52×10^{5}.

Velocity ($m.s^{-1}$)	Density ($kg.m^{-3}$)
15	1.225
Reynold number	**Viscosity ($kg.m^{-1}.s^{-1}$)**
1.52×10^{5}	1.81×10^{-5}

Figure 3: The applied conditions for the numerical calculations in this study.

Figure 4 shows the research plan, which is initialized by creating a background mesh, followed by refining the mesh, running cases in OpenFOAM for various angles of attack and finally carrying out postprocessing.

LITERATURE REVIEW

In terms of the theories used, the fundamental principles of aerodynamics, such as boundary layers and streamlines, are frequently used in this study to explain aerodynamic phenomena.

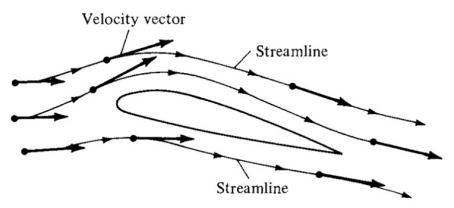

Figure 5: Flow velocity vector and streamline illustration [4]

It is widely acknowledged that the aerodynamic forces and moments acting on an object are attributed to two fundamental sources: the pressure distribution over the surface of the object and the shear stress distribution over the surface of the object. In the case of flow separation, the pressure drag, also called form drag, dominates the total drag, which usually occurs in the flow through a blunt body. Moreover, skin friction drag is especially crucial in the case of a streamlined body.

Moreover, it should be emphasized that there is a marked difference in the pressure distribution between the case of no flow separation and flow separation, which is clearly illustrated in the following picture:

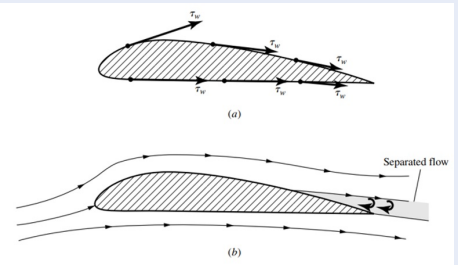

Figure 6: Illustration of (a) shear stress acting on the surface and (b) pressure drag caused by flow separation [4]

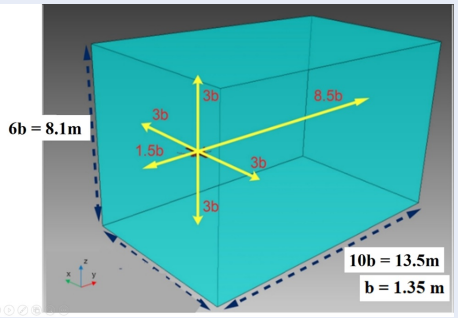

Figure 7: The used box for meshing steps and numerical calculation.

Furthermore, in terms of the stagnation region caused by flow separation, vortices are always present as an evident result of an adverse pressure gradient, especially frequently for a blunt body.

In addition, the vortices are also a consequence of the wing-tip effect, which is illustrated in the following image:

Finally, four aerodynamic coefficients are frequently utilized in this research: the lift coefficient, drag coefficient, pressure coefficient, and skin friction coefficient. These are illustrated in many parts of the numerical results in this research:

Lift coefficient: $C_L = \frac{L}{q_\infty S}$

Drag coefficient: $C_D = \frac{D}{q_\infty S}$

Pressure coefficient: $C_P = \frac{p-p_\infty}{q_\infty}$

Skin friction coefficient: $C_f = \frac{\tau}{q_\infty}$

RESEARCH METHODS

Meshing steps

First, the methodical approach of this numerical study involves placing the examined model in a box

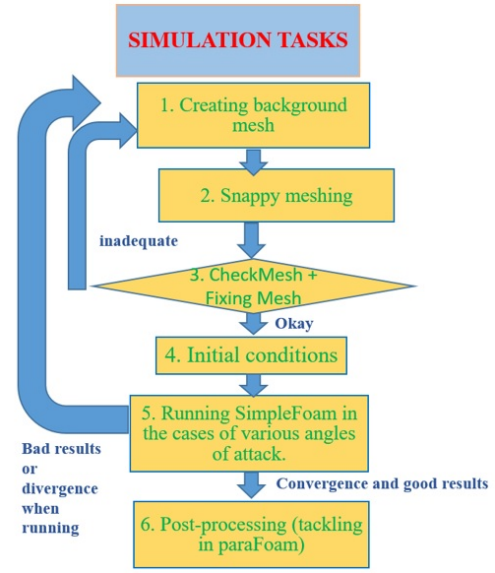

Figure 4: **The plan for this numerical research**.

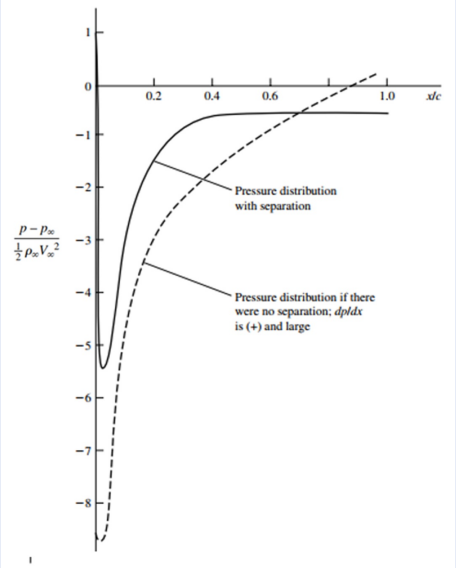

Figure 8: **General view of the pressure distribution difference between two cases: no flow separation and flow separation** [4]

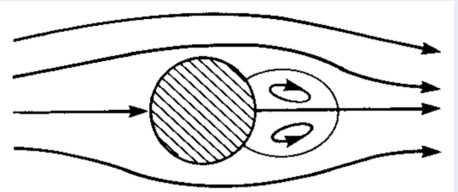

Figure 9: **Occurrence of vortices in the case of a blunt body** [4]

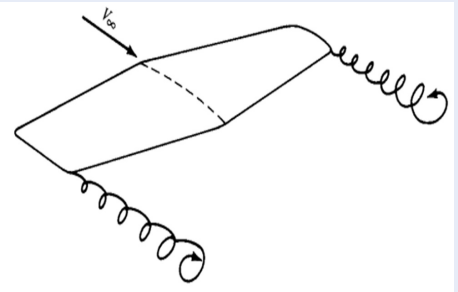

Figure 10: **Illustration of the wing-tip effect** [4]

with dimensions of 6×wingspan, 10×wingspan, and 6×wingspan for lengths of Ox, Oy and Oz, respectively. As mentioned in the introduction, the wingspan of the new model is 1.35 meters. Therefore, in this study, an intentional box was created according to Figure 10. In particular, the distances between the model and the planes (Oxz), (Oxy), and (Oyz) are 1.5×wingspan, 3×wingspan, and 3×wingspan, respectively.

Furthermore, the software SALOME was utilized in this study for the purpose of generating the background mesh because of its evident advantage of interactivity. The process of refining the mesh was subsequently carried out using SnappyHexMesh.

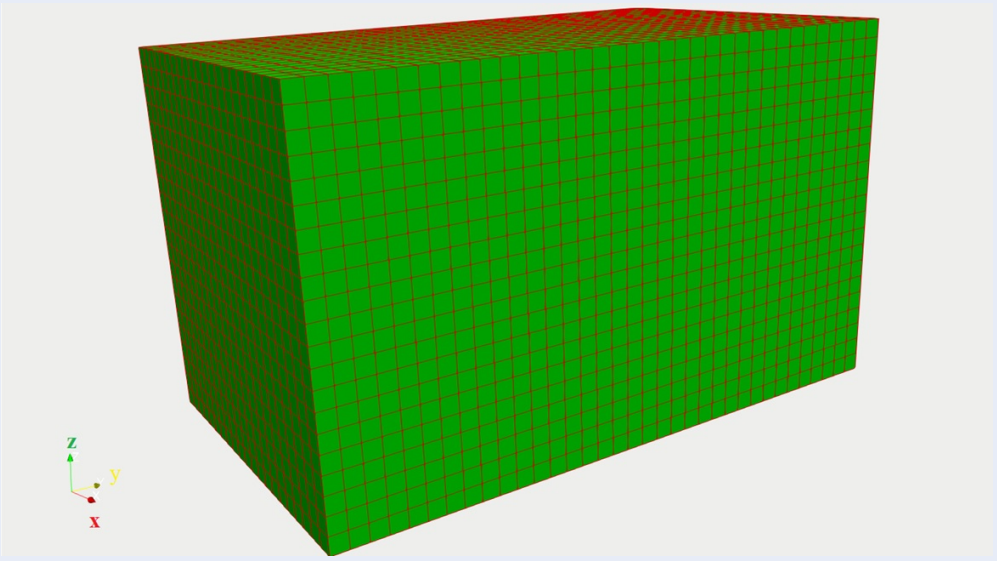

Figure 11: **The background mesh of this study**.

The background mesh was generated so that there was a total of hexahedron cells.

Table 2: Information about the background mesh

Edges	880
Faces	31200
Hexahedrons	360000
% Hexahedrons	100%

In the process of refining the mesh, three boxes were put into the large box at the most important positions, such as at the model position and behind the model. The refining levels are 6, 4 and 3, respectively.

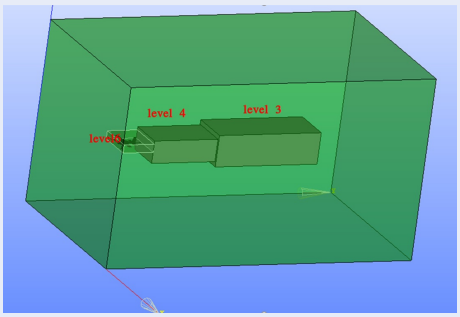

Figure 12: **Putting boxes at the crucial positions of flow through the model for refining meshes.**

After carrying six meshes, two meshes of 16.6 million and 19.4 million are utilized for the final results and for checking the numerical results.

After considering the mesh quality in various aspects, the meshes are appropriate for the next steps of the numerical calculation.

Preprocessing

In our research, the chosen turbulence model was k-ω-SST, which belongs to the turbulence-calculation approach RANS because it is adequate for our numerical resource conditions.

Figure 17 illustrates the necessary directories for the turbulence model k-ω-SST in OpenFOAM. In turn, the condition and specification were inputted in different directories in the direction set for the k-ω-SST model. As introduced earlier, the research intention is to investigate the aerodynamic characteristics of the model at various angles of attack. As a result, the lift direction, drag direction and wind direction should be changed for each angle of attack.

For the normal condition of the free airstream, the turbulence intensity is approximately 0.1% to 0.2%. In this research, a turbulence intensity of 0.2% was chosen to set up the initial conditions. The values of k and ω were calculated as follows:

$$k = \frac{3}{2}(UI)^2 = \frac{3}{2}(15 * 0.002)^2 = 0.00135\ m^2/s^2$$

l = 0.07 × c = 0.0105 m

$$\omega = \frac{k^{0.5}}{C_\mu^{0.25} * l} = \frac{0.00135^{0.5}}{0.09^{0.25} * 0.0105} = 6.38876565\ s^{-1}$$

Table 3: The refined mesh utilized for the final results and for checking the numerical results

Meshes used for the final results	Mesh IV	Mesh V (for checking results)
Cell number of the background mesh	376 thousand	376 thousand
Cell number of the refined mesh	16.6 million	19.4 million
Aspect ratio	98.8	98.8
Non-orthogonality	4.66	4.51
Max. Skewness	3.32	3.3
1^{st} layer thickness	$2.5x10^{-5}$	$2.5x10^{-5}$
Number of layers	8.36	8.37
Total layer thickness	1.38mm, represents 76.5% desired thickness	1.38mm, represents 76.5% desired thickness

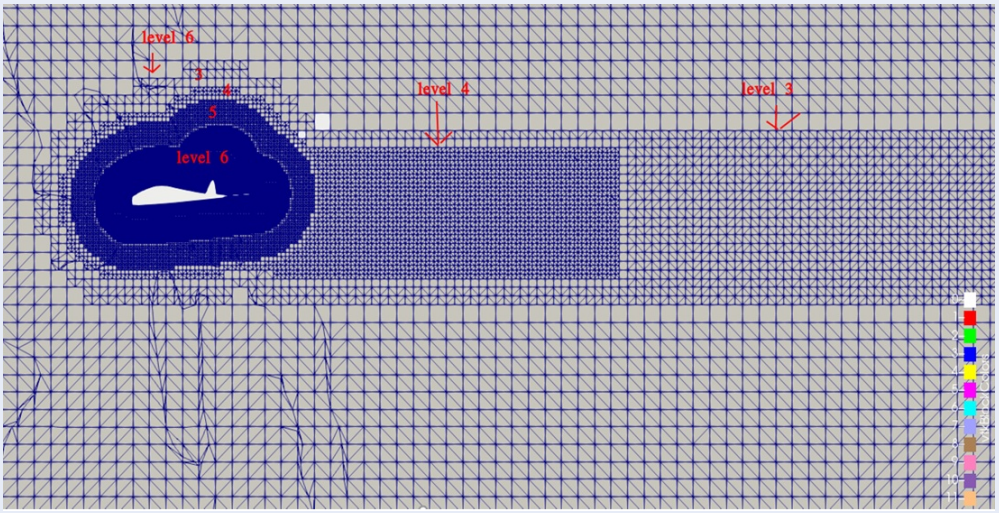

Figure 13: The refining levels in the surrounding regions of the model.

Afterwards, those values were input into the k and ω directories in the k-ω-SST directory set.

In terms of boundary conditions, the type of *wall* was chosen as *noSlip,* while the *inlet* and *outlet* were selected as *fixedValue* and *inletOutlet,* respectively. The input information is presented in the following image and table:

SIMULATION ANALYSIS RESULTS

There are seven types of numerical results in this research, including residual convergence charts, lift coefficient versus angle of attack, drag coefficient versus angle of attack, lift-to-drag ratio versus angle of attack, pressure coefficient, skin-friction coefficient, and illustrations of the flow field.

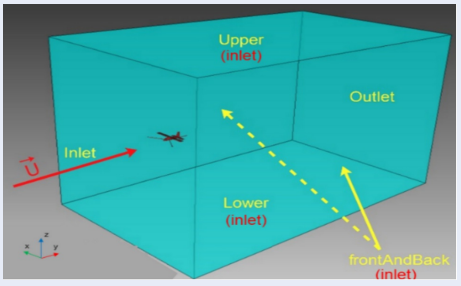

Figure 18: The boundary conditions in this study.

Residual convergence

First, the residual charts converge fairly well at angles of attack lower than 12 degrees, but above that angle of

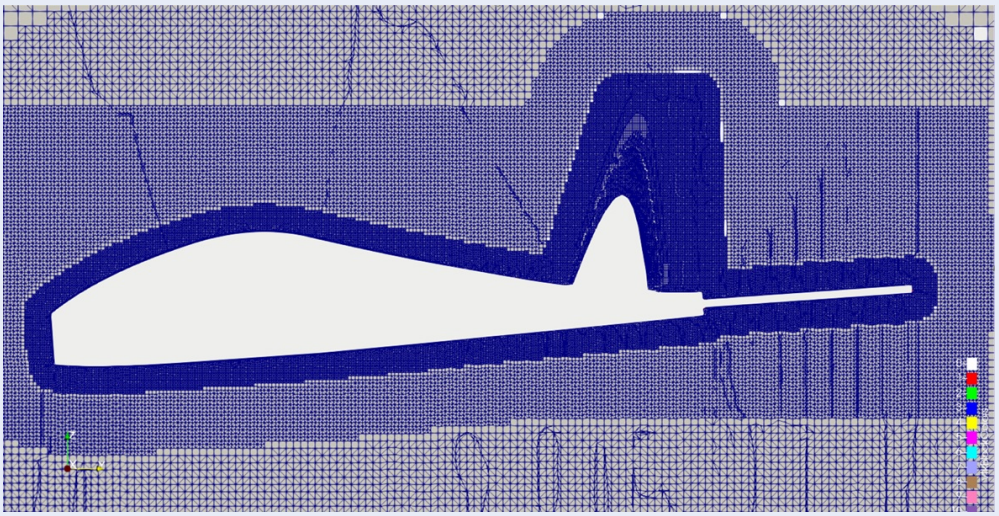

Figure 14: **Refined mesh adjacent to the surface of the model**.

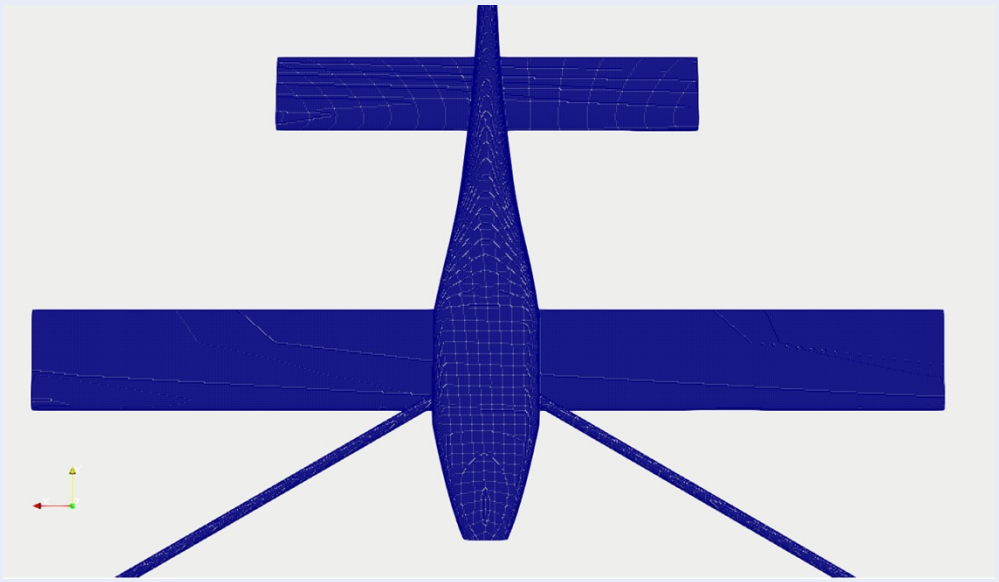

Figure 15: **The refined mesh on the lower surface**.

Table 4: **Information on the boundary conditions**

Patches	Type of boundary condition in OpenFOAM
Wall (HOPE model)	type noSlip;
inlet	type fixedValue;
outlet	type inletOutlet; inletValue uniform (0 0 0);

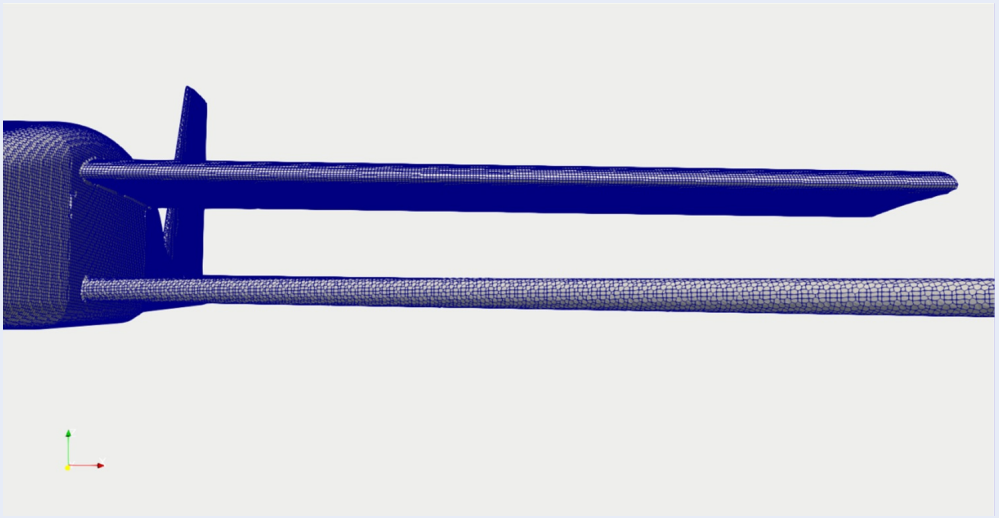

Figure 16: **Refined mesh on the wing and bar.**

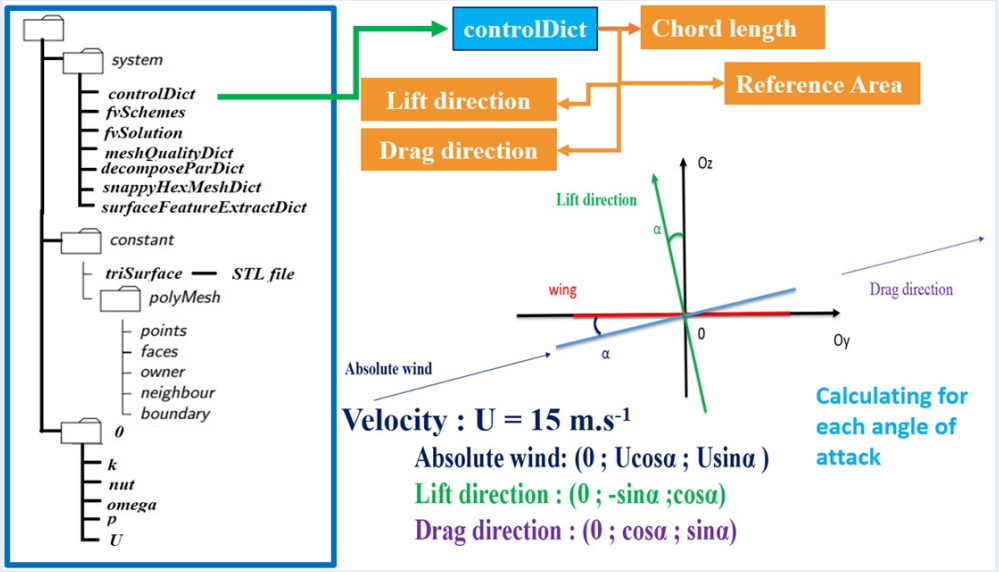

Figure 17: **Inputting the initial conditions for the turbulence model k-ω-SST.**

attack, the residual charts fluctuate remarkably. This occurrence of strong fluctuation is certainly due to the flow separation. The flow separation at a high angle of attack will be discussed in the following section.

Lift coefficient versus angle of attack

The following results are the lift coefficients of the two-dimensional airfoil typed BE12355d, the Huynh Tri Pham model[2] and the Thanh Duc Nguyen model[1]. There are some considerable points in this chart, which are that the zero-lift angle of attack of the new model (T.D.Nguyen model executed in this research) is minus 3 degrees. The lift-slope of this new model is 0.0778. The maximum lift coefficient is approximately 0.92 at an angle of attack of 14 degrees. Moreover, it is easy to recognize that the two executed meshes give almost the same results, which proves the accuracy of the numerical results independent of the mesh cell number.

Table 3 shows a comparison of the important parameters of the two-dimensional airfoil, H.T. Pham model and T.D. Nguyen model.

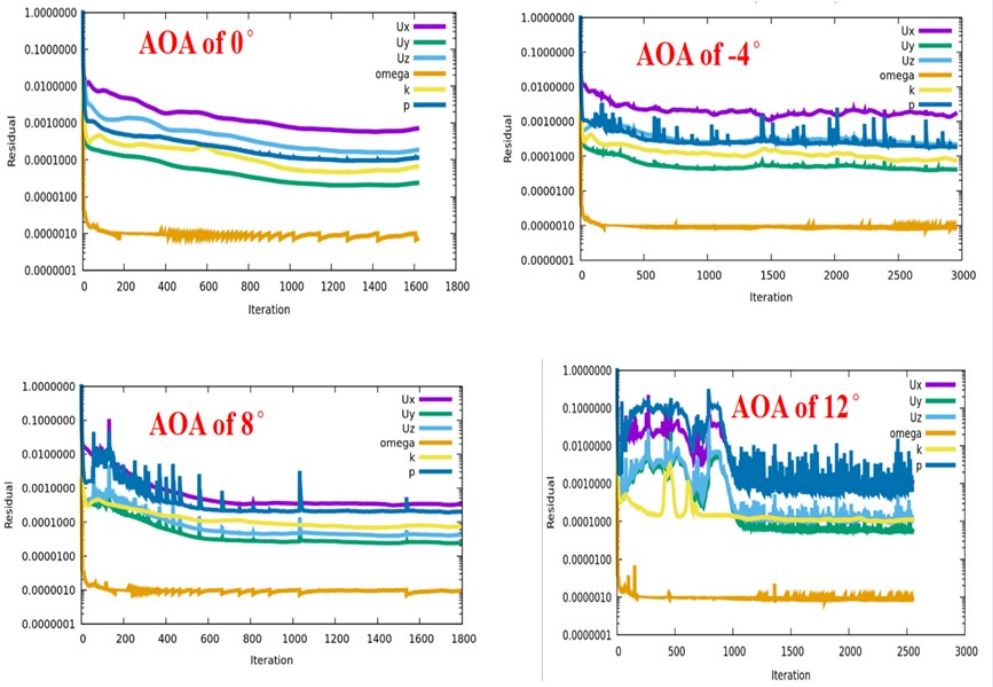

Figure 19: **Residual convergence charts**.

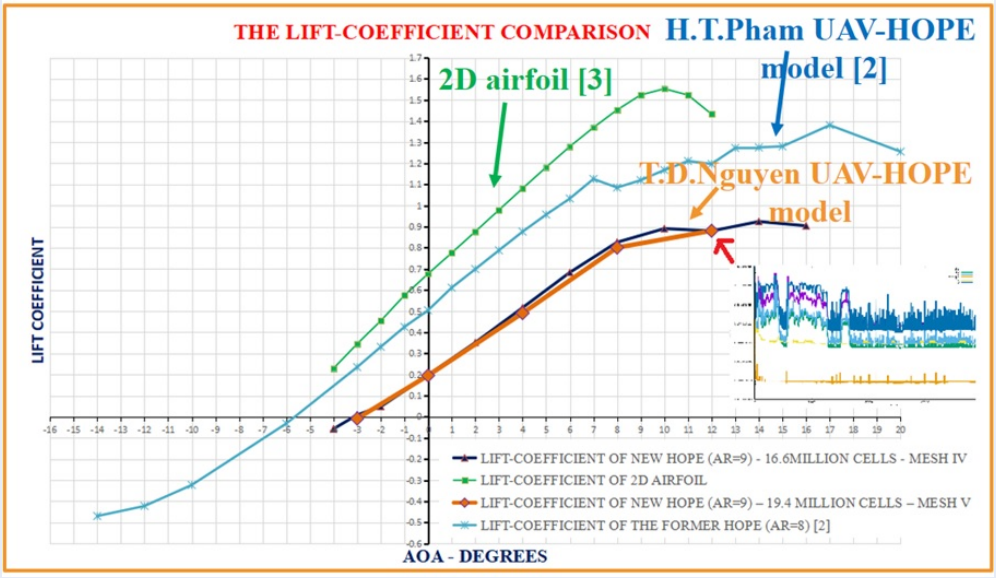

Figure 20: **Lift coefficient comparison of the two-dimensional airfoil, H.T. Pham model and T.D. Nguyen model.**

Table 5: Comparison of the aerodynamic factors of these objects

Factors	2D airfoil	The UAV-HOPE model - P.H.Tri 2015	The new UAV-HOPE model - N.T.Duc 2018
Life slope	0.0989	0.0888	0.0778
Zero-lift angle of attack	-6^o	-5.7^o	-3^o
Lift coefficient at AOA of 0^o	0.6768	0.5039	0.1974

In comparison, in the case of cruising between two models, the lift-to-takeoffweight is slightly increased in the latter model.

Following the aerodynamic relationship between the maximum lift coefficient $C_{L,max}$ and V_{stall}, the stall velocity can be determined for the new model (the N.T.Duc model) as follows:

$$V_{stall} = \sqrt{\frac{2W}{\rho_\infty S C_{L,max}}} = \sqrt{\frac{2\times3\times9.81}{1.225\times0.2025\times0.9243}} = 17.3\ m/s$$

where S is the wing area of 0.2025 m^2

W is the take-off weight of 3.5 kg.

Drag coefficient versus angle of attack

For a zero-lift angle of attack of -3°, the zero-lift drag coefficient is 0.146. The minimum drag coefficient is 0.12 at an angle of attack of 0°.

With a minimum drag coefficient $C_{D,min}$ of 0.12, the relationship between the maximum velocity and the maximum thrust for the T.D.Nguyen model is:

$$V_{max} = \sqrt{\frac{2\times T_{max}}{\rho_\infty S C_{D,min}}} = \sqrt{\frac{T_{max}}{0.0149}}$$

where T_{max} is in units of meters.

Lift-to-drag ratio versus angle of attack

The maximum lift-to-drag ratio is also shown in Figure 22. As illustrated clearly, the maximum lift-to-drag ratio is approximately 5.38 for the new model (T.D.Nguyen model) at an angle of attack of 8.

Pressure coefficient

In the two next types of results, which are the pressure coefficient and skin friction coefficient, the two types of coefficients are shown in the most special positions on the wing. Those positions include seven twelfth wingspans, three fourth wingspans, and eleven twelfth wingspans. In addition, two cases of no flow separation at an angle of attack of 0° and flow separation at an angle of attack of 16° are shown.

At an angle of attack of 0° (no flow separation),

In this case, the pressure coefficient on the upper surface decreases significantly to the minimum value at approximately 0.18 chord length and then increases gradually to approximately 0 at the trailing edge.

At an angle of attack of 16° (occurrence of flow separation):

Unlike in the former case, in this case, the pressure coefficients on the upper surface are all negative, particularly from -1.5, increasing gradually to -0.4 at the trailing edge. Moreover, the pressure coefficient on the lower surface decreases significantly from 0.9 to -0.4.

Skin friction coefficient

At an angle of attack of 0° (no flow separation),

In terms of the skin friction coefficient, at an angle of attack of 0°, the upper surface has higher values than the lower surface from the leading edge to approximately three fourths of the chord length.

At an angle of attack of 16° (occurrence of flow separation):

In contrast, at an angle of attack of 16°, where there is already flow separation, the skin friction coefficient on the upper surface is lower than that on the lower surface for most of the wing chord.

Flow field

Velocity field

As shown in Figure 30, there is a stagnation region on the wing at an angle of attack of 16°, where there is no velocity.

Pressure field

It is clear that there is a region with the highest pressure at the leading edge of the wing slice. Widely accepted knowledge is the stagnation region of a wing.

Table 6: Lift-to-takeoffweight comparison

The former UAV-HOPE model - P.H.Tri 2015	The new UAV-HOPE model - N.T.Duc 2018
At the angle of attack of 0^o (cruising), $C_L = 0.5039$	At the angle of attack of 4^o (cruising), $C_L = 0.5164$
$L = 0.5 \times C_L \times V^2 \times S \times \rho$	$L = 0.5 \times C_L \times V^2 \times S \times \rho$
$L = 0.5 \times 0.5039 \times 15^2 \times 0.18 \times 1.225$	$L = 0.5 \times 0.5164 \times 15^2 \times 0.2025 \times 1.225$
$L = 12.5\ N$	$L = 14.41\ N$
$\frac{L}{W} = \frac{12.5 \times 100\%}{3.5 \times 9.81} = 36.41\%$	$\frac{L}{W} = \frac{14.41 \times 100\%}{3.5 \times 9.81} = 41.97\%$

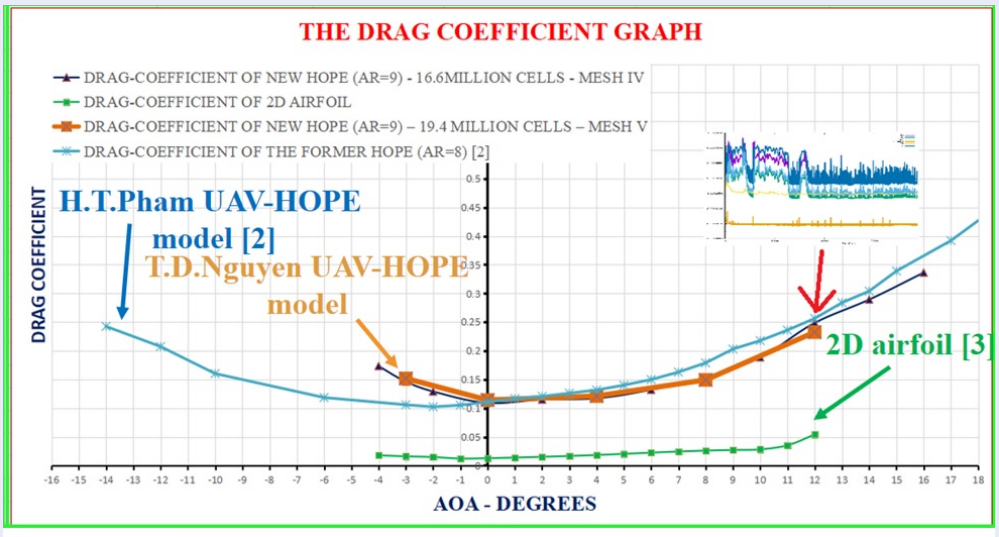

Figure 21: **Drag coefficient comparison of the two-dimensional airfoil, H.Tri.Pham model [2], and T.D.Nguyen model [1]**

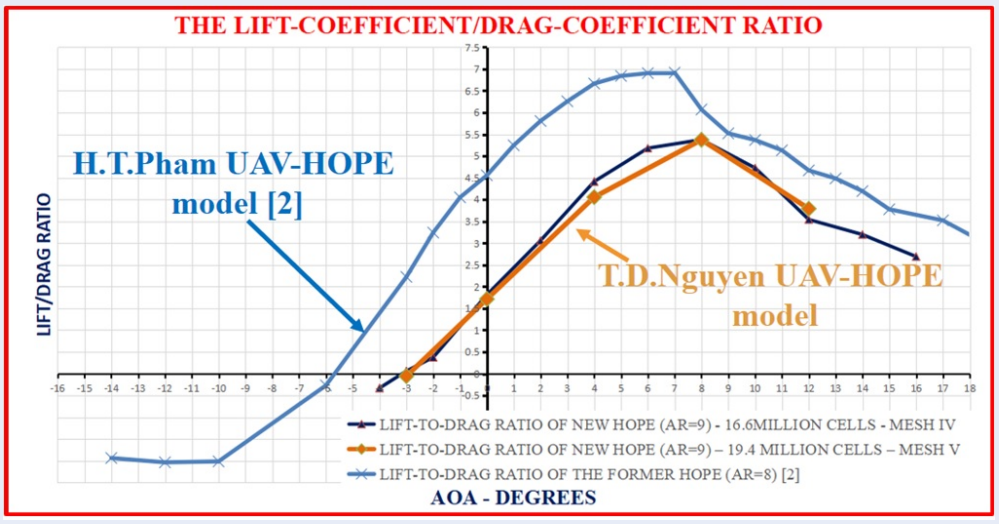

Figure 22: **The lift-to-drag ratio of the two models.**

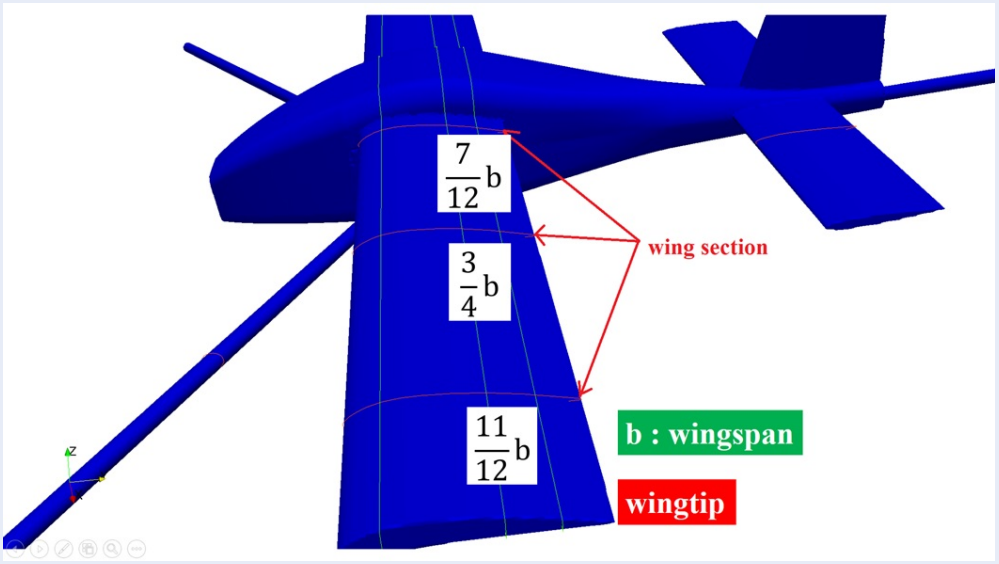

Figure 23: **Special positions on the wing to examine the pressure coefficient and skin friction coefficient.**

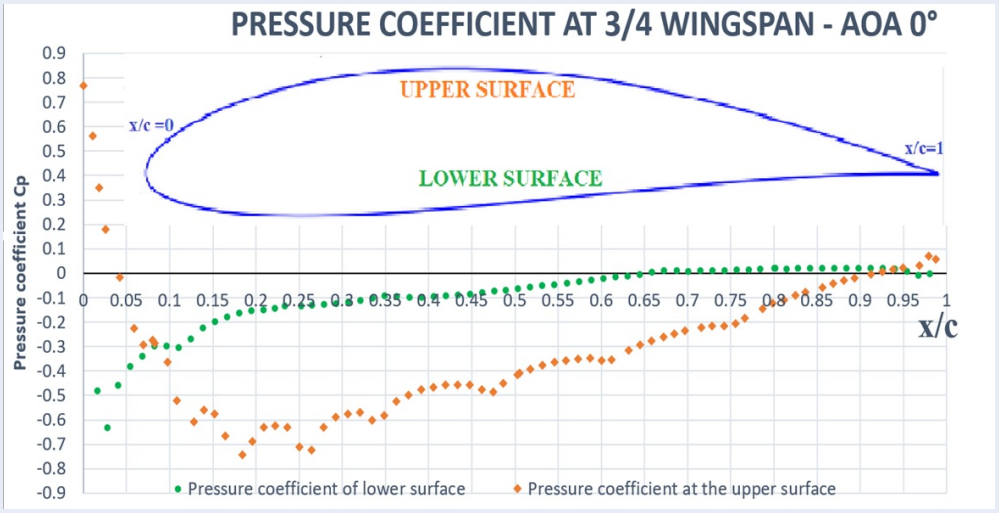

Figure 24: **Pressure coefficient at the three fourth wingspans at an angle of attack of 0°.**

Wingtip vortex

Vortex in the stagnation region

Figure 33 clearly illustrates the vortex in the stagnation region, which is caused by the adverse velocity gradient.

The y^+ field

As a factual requirement of the turbulence model k-ω-SST, the y^+ on the surface of the model should be 1. As shown in Figure 34 and Figure 35, y^+ is approximately 1 for most of the model, except for the outside parts of the vertical stabilizers. This is also the factor for ensuring the accuracy of the numerical results in this study.

CONCLUSION

This study successfully described the entire process of numerical calculation and simulation for a three-dimensional model with the most popular turbulence model, k-ω-SST, in the case of a quite low Reynolds number. Moreover, the research also illustrated the crucial aerodynamic properties of this model through graphs of aerodynamic coefficients such as the lift co-

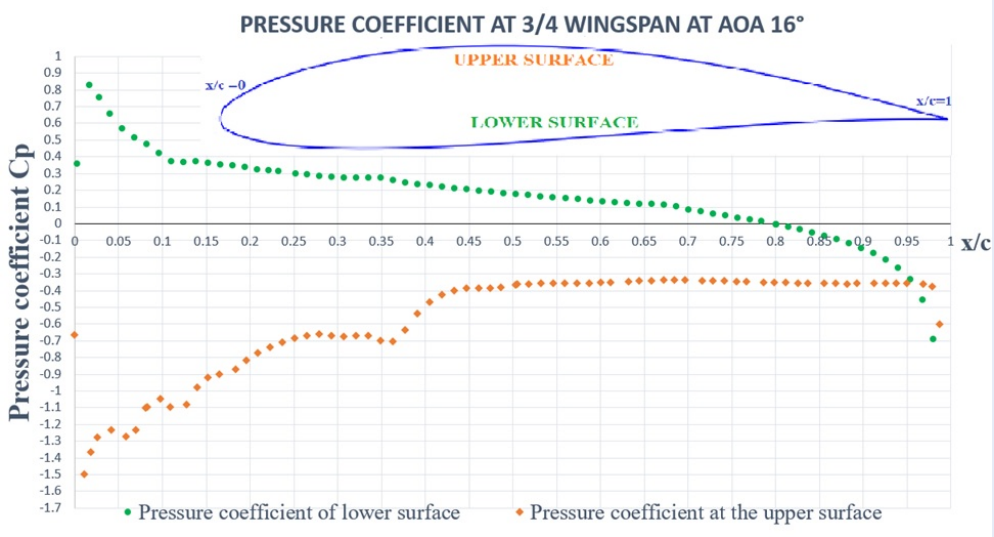

Figure 25: **Pressure coefficient at the three fourth wingspans at an angle of attack of 16°.**

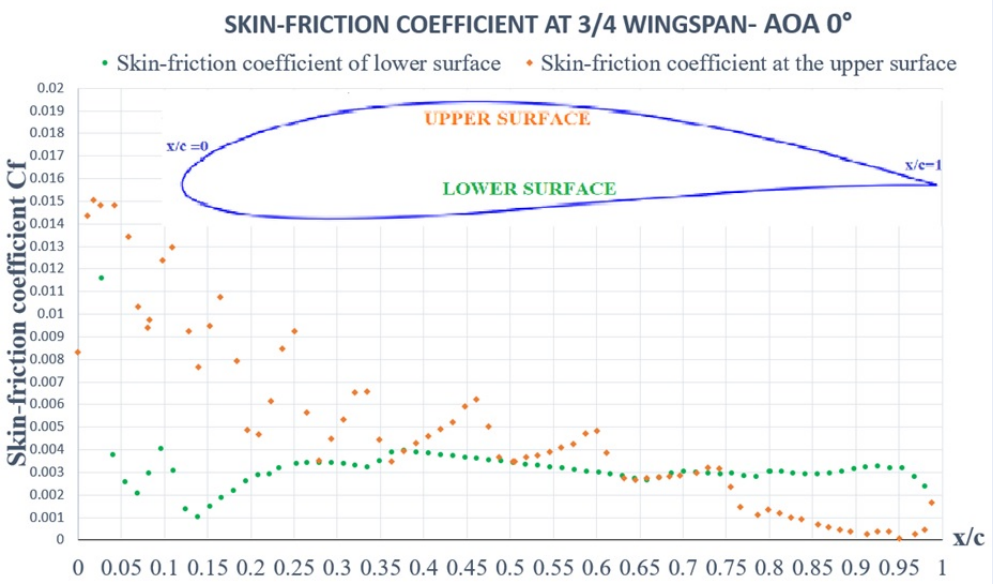

Figure 26: **Skin friction coefficient at the three fourth wingspans at an angle of attack of 0°.**

efficient, drag coefficient, and lift-to-drag versus the angle of attack. In addition, the pressure coefficient and skin friction coefficient are also described at the most special positions on the wing to provide a clear view of the aerodynamic properties. Furthermore, this study has estimated several performance parameters, such as the lift slope, the zero-lift angle of attack, the zero-lift drag coefficient, the maximum lift coefficient, and the minimum drag coefficient. Ultimately, the study numerically demonstrated the various fields, including the velocity field, pressure field, and vortices for the wingtip effect and in the stagnation region. It is hoped that the authors will be able to identify the special structure of Laminar Separation Buble (LSP) when Renoyld's number is low, as in this study, in the near future.

ABBREVIATIONS

None.

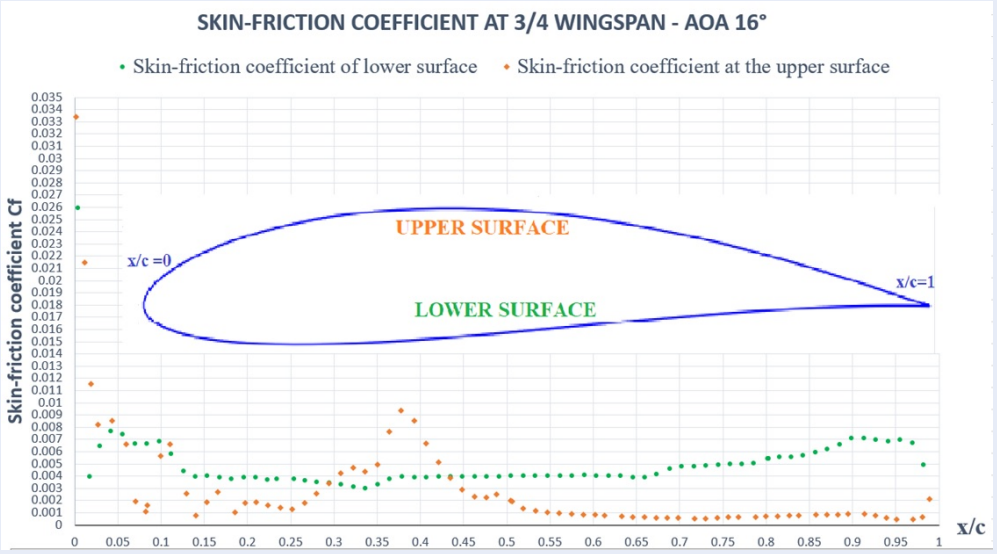

Figure 27: **Skin friction coefficient at the three fourth wingspans at an angle of attack of 16°.**

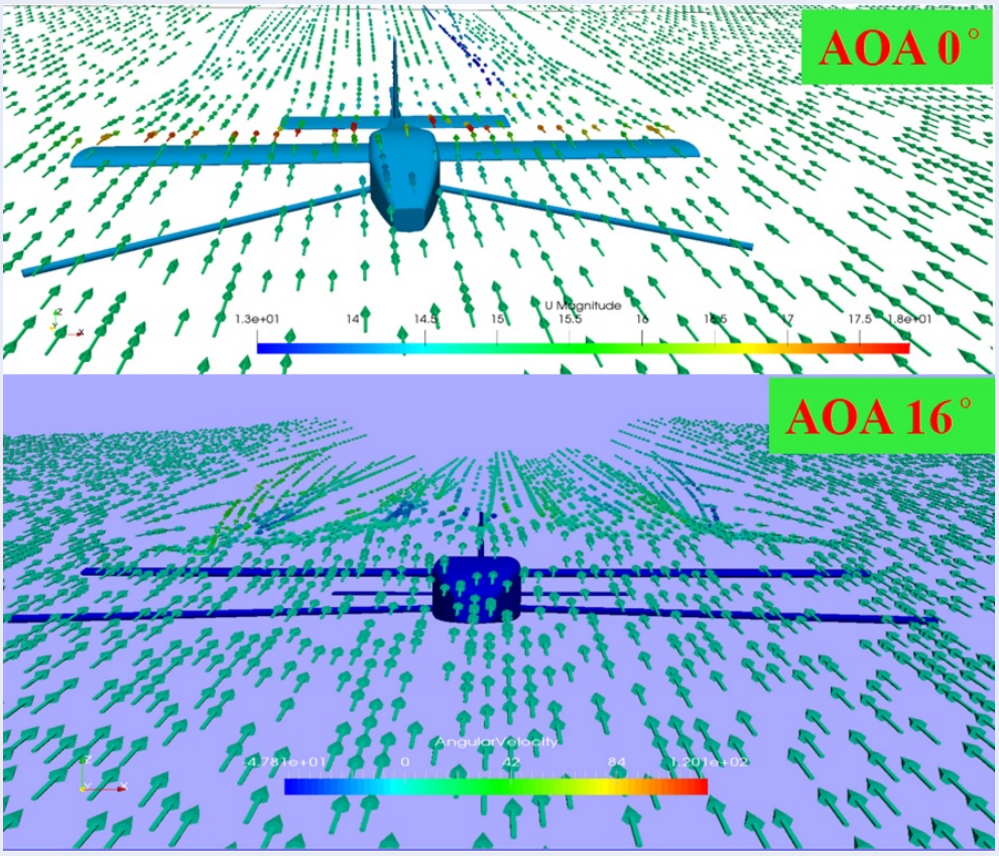

Figure 28: **The velocity field shown at angles of attack of 0° and 16°.**

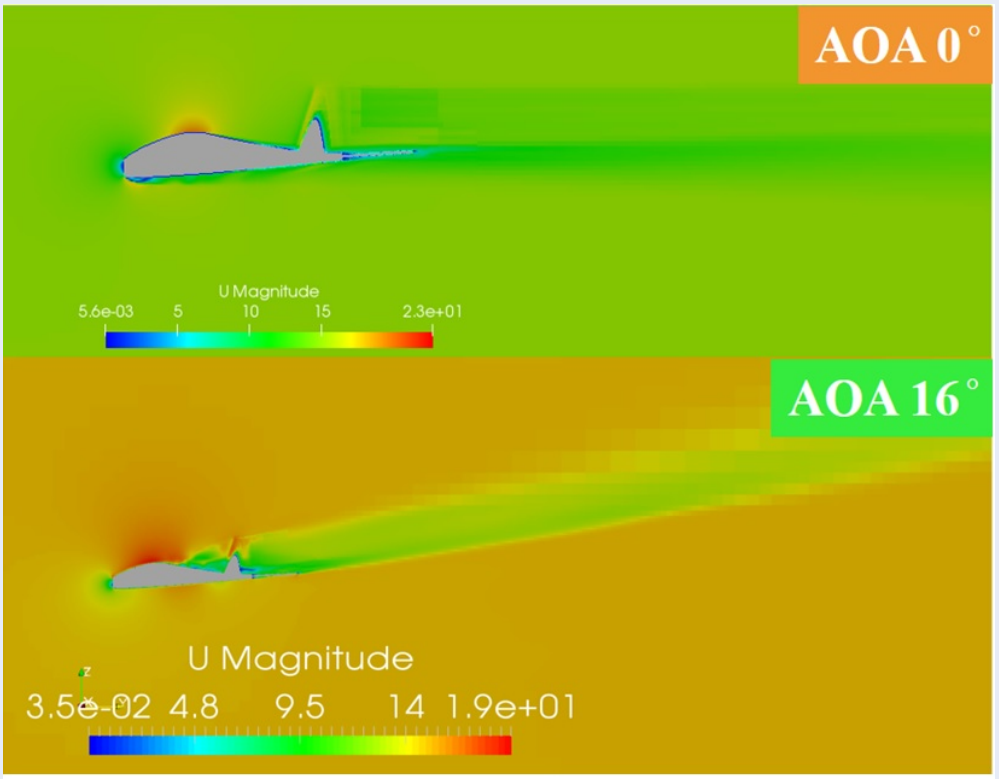

Figure 29: **Different viewpoints of the velocity field at angles of attack of 0° and 16°.**

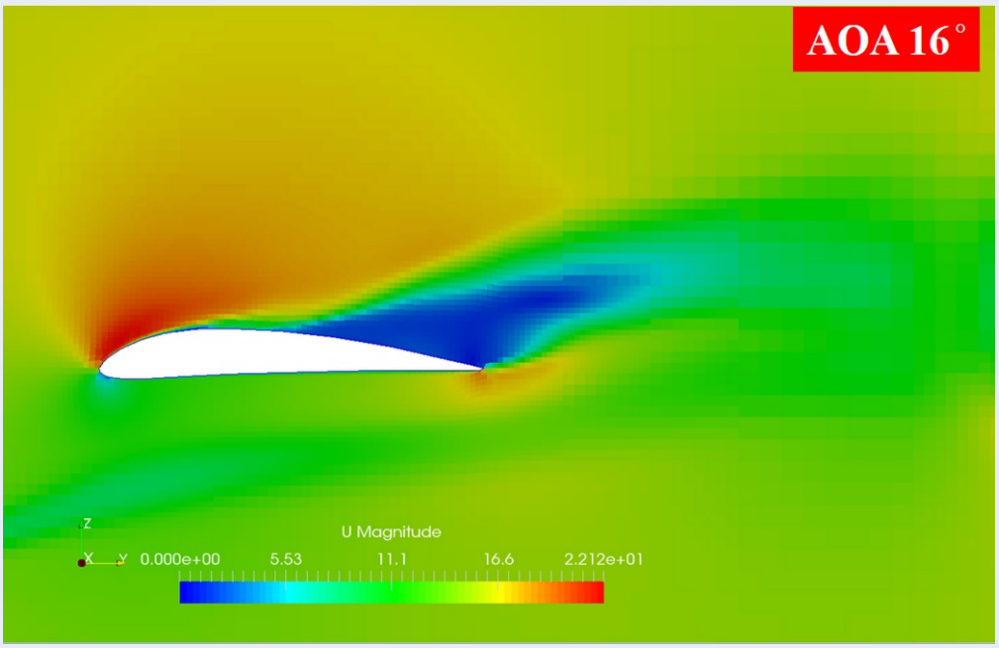

Figure 30: **The stagnation region at an angle of attack of 16°.**

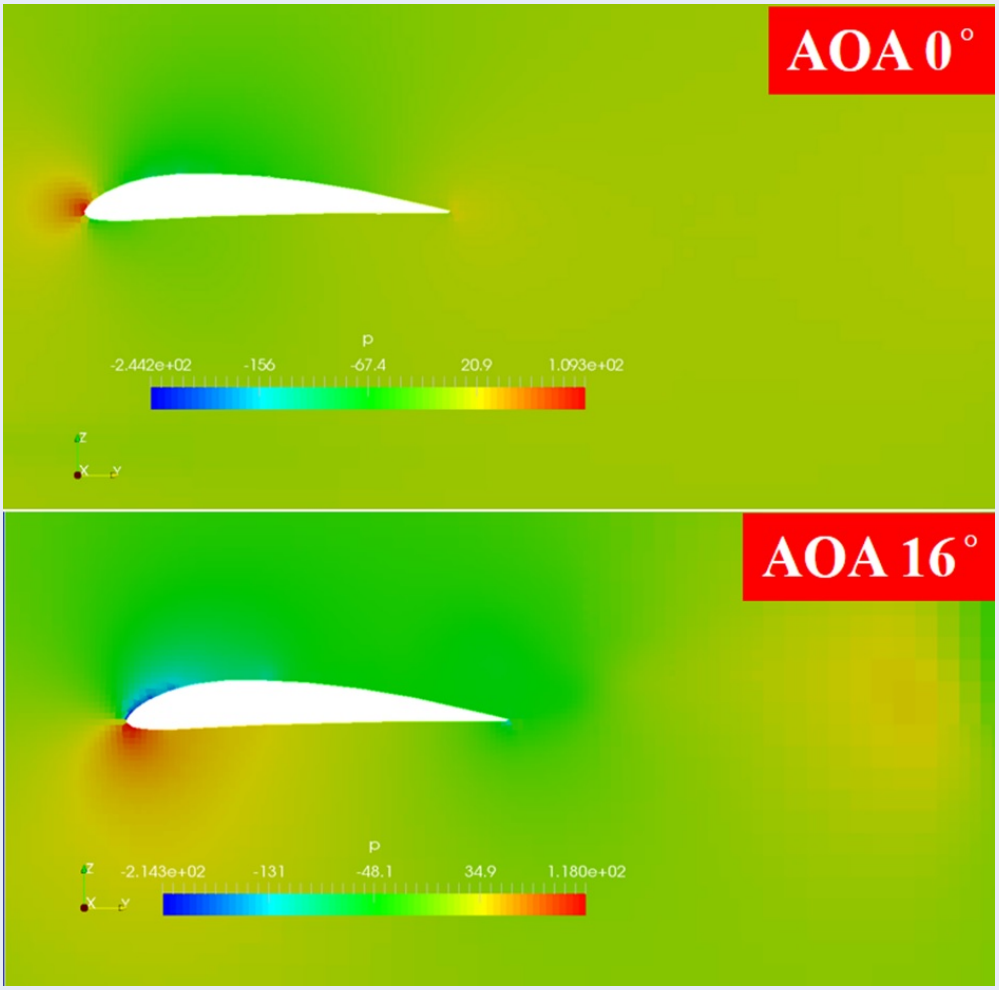

Figure 31: **The pressure field at angles of attack of 0° and 16°.**

ACKNOWLEDGMENTS

None.

FUNDING

None.

AUTHORS' CONTRIBUTIONS

All authors significantly contributed to this work. All authors read and approved the final manuscript.

CONFLICT OF INTEREST

The authors declare that they have no competing interests.

REFERENCES

1. Duc NT. Thiết kế kết cấu và chế tạo máy bay UAV bằng vật liệu Composite (Phần kết cấu cánh) [graduation thesis]. Ho Chi Minh City: Ho Chi Minh City University of Technology; 2018;.
2. Tri PH. Design a VTOL UAV - stability analysis & 3D simulation [graduation thesis]. Ho Chi Minh City: Ho Chi Minh City University of Technology; 2015;.
3. Huynh TTX. Tính toán và mô phỏng số cho máy bay UAV kết hợp cánh bằng và ba chong chóng (HOPE) bằng phần mềm OpenFOAM [graduation thesis]. Ho Chi Minh: Ho Chi Minh City University of Technology; 2018;.
4. John J, Anderson D. Fundamentals of aerodynamics. 5th ed, McGrall-Hill; 2011;.

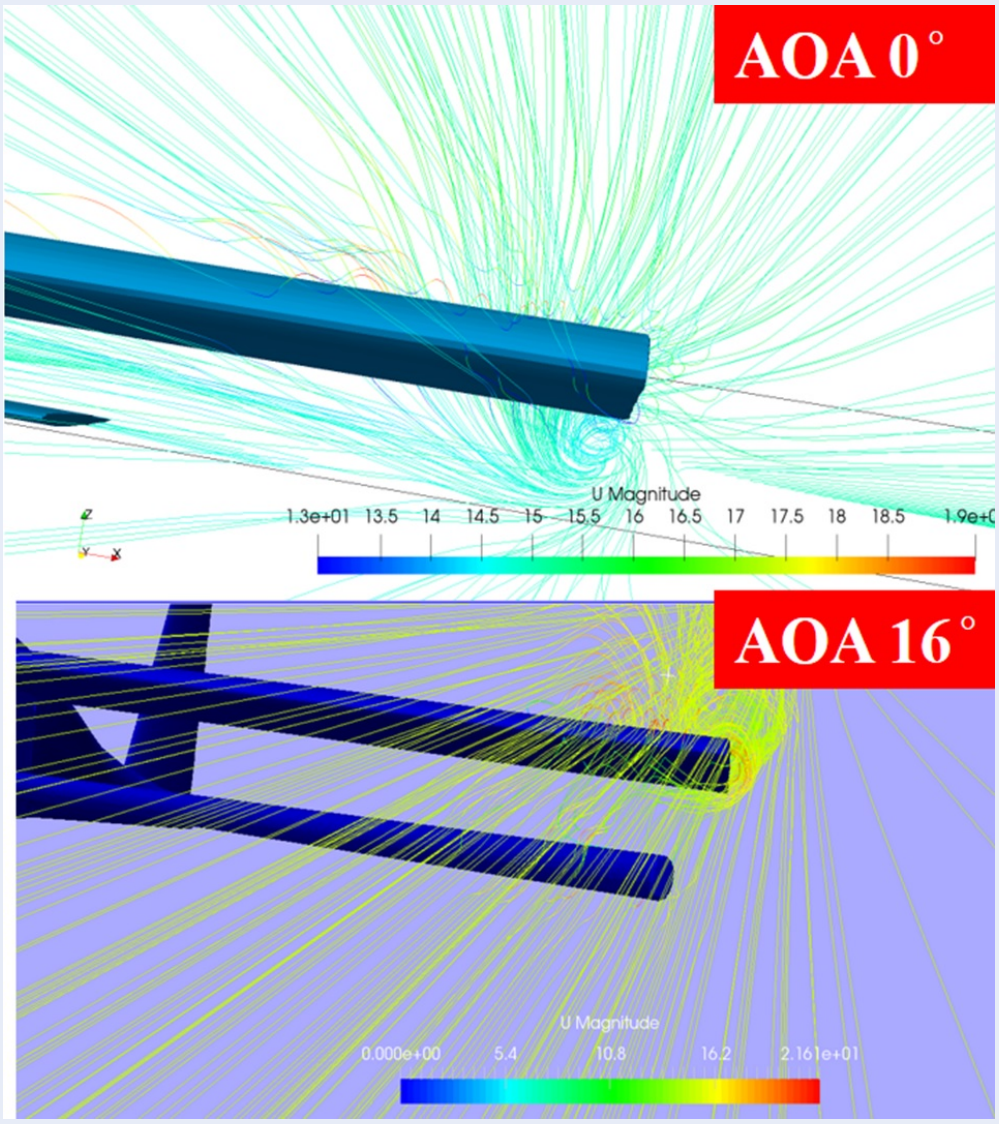

Figure 32: **The wingtip vortices at angles of attack of 0° and 16°.**

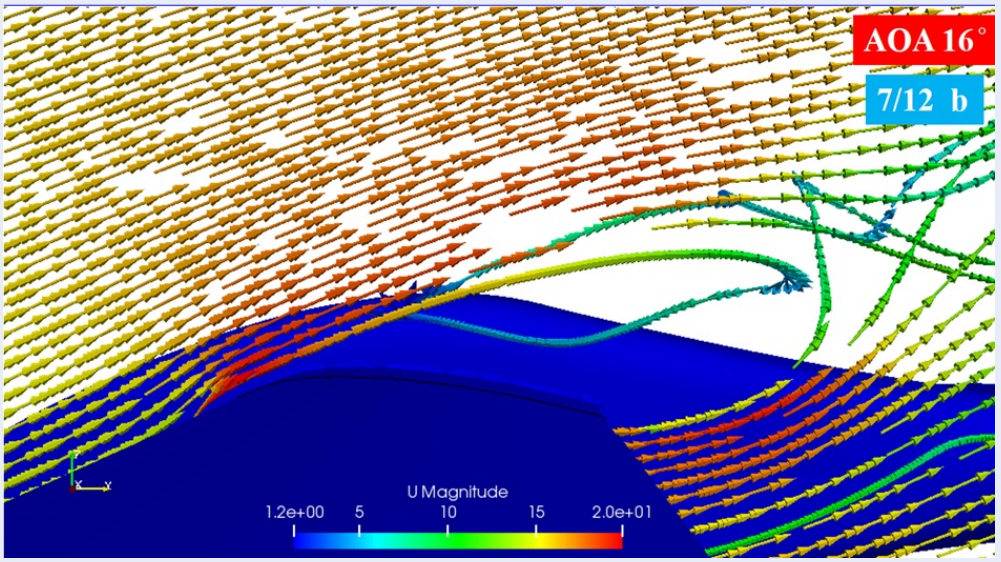

Figure 33: **Vortex in the stagnation region.**

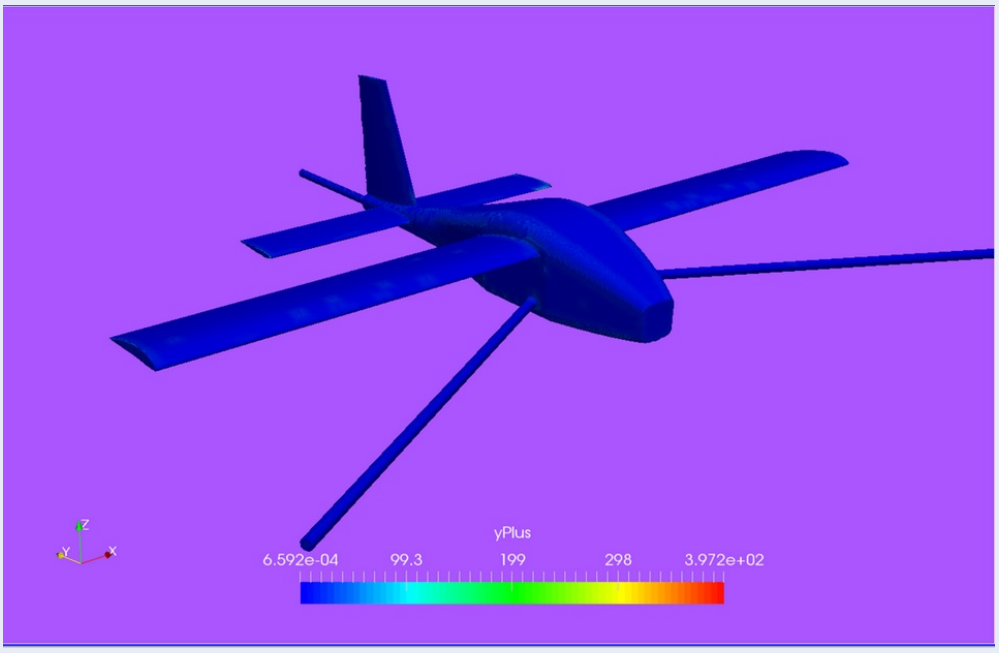

Figure 34: **y^+ values on the surface of the model.**

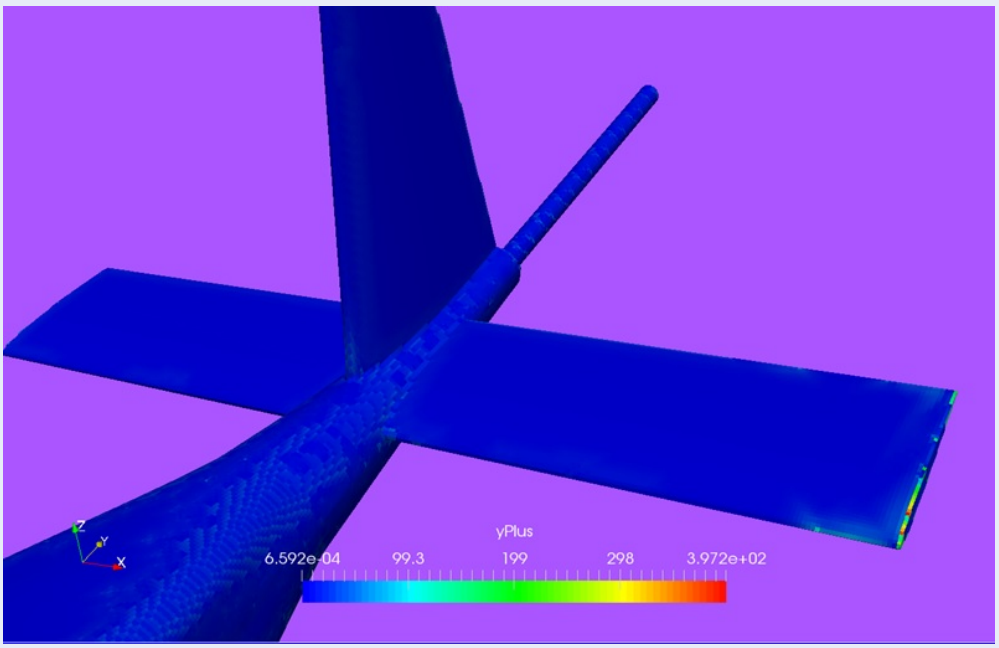

Figure 35: y^+ values on the surface of the model tail.